DOI: 10.3901/CJME.2015.0318.033, available online at www.cjmenet.com; www.cjme.com.cn

Interaction of In-wheel Permanent Magnet Synchronous Motor with Tire Dynamics

SONG Ziyou, LI Jianqiu, WEI Yintao, XU Liangfei, and OUYANG Minggao*

State Key Laboratory of Automotive Safety and Energy, Tsinghua University, Beijing 100084, China

Received September 5, 2014; revised March 11, 2015; accepted March 18, 2015

Abstract: Drive wheel systems combined with the in-wheel permanent magnet synchronous motor (I-PMSM) and the tire are highly electromechanical-coupled. However, the deformation dynamics of this system, which may influence the system performance, is neglected in most existing literatures. For this reason, a deformable tire and a detailed I-PMSM are modeled using Matlab/Simulink. Furthermore, the influence of tire/road contact interface is accurately described by the non-linear relaxation length-based model and magic formula pragmatic model. The drive wheel model used in this paper is closer to that of a real tire in contrast to the rigid tire model which is widely used. Based on the near-precise model mentioned above, the sensitivity of the dynamic tire and I-PMSM parameters to the relative error of slip ratio estimation is analyzed. Additionally, the torsional and longitudinal vibrations of the drive wheel are presented both in time and frequency domains when a quarter vehicle is started under conditions of a specific torque curve, which includes an abrupt torque change from 30 N • m to 200 N • m. The parameters sensitivity on drive wheel vibrations is also studied, and the parameters include the mass distribution ratio of tire, the tire torsional stiffness, the tire damping coefficient, and the hysteresis band of the PMSM current control algorithm. Finally, different target torque curves are compared in the simulation, which shows that the estimation error of the slip ratio gets violent, and the longitudinal force includes more fluctuation components with the increasing change rate of the torque. This paper analyzes the influence of the drive wheel deformation on the vehicle dynamic control, and provides useful information regarding the electric vehicle traction control.

Keywords: I-PMSM, tire dynamics, slip ratio estimation, tire torsional vibrations, longitudinal vibrations

1 Introduction

In-wheel permanent magnet synchronous motors (I-PMSMs) are widely used in electric vehicles (EVs) to realize a more flexible vehicle dynamic control effect[1–2]. With regard to the PMSM control, the field-oriented control (FOC) algorithm is used in this study relying on its good performance for ripple-free torque production[3]. The I-PMSM and tire in the drive wheel system are highly electromechanical-coupled; however, most of the published research regarding the in-wheel-motored EV control is on the basis of simplified rigid wheel dynamics models[4–6]. As a result, the different dynamic properties that are caused by different parameters of the I-PMSM and tire cannot be sufficiently captured when the rigid wheel assumption is adopted. In particular, for aggressive driving/braking events, the errors introduced by tire torsional dynamics may significantly affect the traction control performance. From this standpoint, various deformable tire models have been developed to better approximate the transient dynamics of tires[7–8]. In this study, a rigid ring (deformable tire) model was used due to its simplicity and accuracy[9–10], furthermore, the tire/road contact interface is accurately described by the non-linear relaxation length-based model[11] and Magic Formula pragmatic model[12].

Tire-ABS interaction has attracted much attention and it has been demonstrated that tire transient dynamics has a significant influence on anti-lock brake system (ABS) performance[13–15]. The basic reason for this is the deformation and vibration of tires during instantaneous dynamic motions, e.g., severe acceleration or braking cases. This will bring a distinction between the variables of rotor/hubs and tire rings, including the rotary position and rotary velocity. It introduces a slip ratio estimation error as the rotor/hub's rotary velocity is used in the slip ratio estimation, which is very important in many applications, such as vehicle traction control[16–17] and electronic differential algorithm[18], etc. Thus it is of great significance to consider the influence of the error introduced by tire deformation and to investigate methods of matching the parameters of the drive wheel to reduce the estimation error of slip ratio.

Various parameters of the drive wheel also bring distinguishing effects of tire torsional and longitudinal vibrations during acceleration/brake processes. In

* Corresponding author. E-mail: ouymg@tsinghua.edu.cn
Supported by National Natural Science Foundation of China (Grant Nos. 51275265, 51175286), and National Hi-tech Research and Development Program of China (863 Program, Grant No. 2012DFA81190)

conventional vehicles, the driveline consists mainly of engine, torque converter or clutch, transmission system, driveshaft, differential, half-shafts, and wheels, which are all elastic in nature. As a result, the presence of the torque converter or clutch, together with the driveline system's elastic nature, provides a passive way of damping the vibration in the driveline of a conventional vehicle when it is subjected to either acceleration or deceleration. However, wheel-independent-drive EVs have inherent low damping in their drivelines since they use rotors to directly connect the tire hub, thus lacking a clutch or a torque converter that provides the conventional vehicle with driveline damping effect[19]. The driveline in a wheel-independent-drive EV is more rigid (i.e., less elastic) due to the direct mechanical coupling between the motor and the tire hub. In addition, electric motors input faster torques to the tire hub, which implies a more severe stimulation to the tire and the tire/road interface. Finally, the vibration in the drive wheel system of wheel-independent-drive EVs cannot be neglected. To ensure that the vibration frequency of the drive wheel is away from the natural frequency of the powertrain lines and chassis, these vibrations should be analyzed both in the time and frequency domains[20].

In light of the above, this paper models a quarter in-wheel-motored vehicle to study the interaction between I-PMSMs and tires with different component parameters under specific start/acceleration conditions. The regulation regarding the influence of the various parameters on the slip ratio estimation error is schematically shown in two map diagrams, which can assist engineers to match the I-PMSM and tire parameters to reduce the estimation error. Having an accurate slip ratio will improve the traction control effects. Beyond that, the impact of different parameters on tire vibrations is investigated both in the time and frequency domains. This enables us to have a better understanding of the vibration frequency range of the drive wheel, and benefits the parametric matching work to avoid the resonant vibration occurrence. Based on the typical system composed of a typical tire and a typical I-PMSM, different target torque curves of the I-PMSM are compared in the simulation and the results are instructional to the EV traction control algorithm.

The rest of this paper is organized as follows. Firstly, the model of a quarter EV is briefly described. Secondly, the estimation error of slip ratio is analyzed, and the drive wheel vibrations are presented both in time and frequency domains for different parametric conditions. Several conclusions are also discussed. Thirdly, the vehicle performance under four different torque curves are compared and analyzed. Finally, several conclusions are drawn.

2 Quarter EV Model

2.1 I-PMSM model[21–24]

The following assumptions are made before establishing the mathematical model of I-PMSM:

(1) Neglects the saturation of the electric motor ferrite core.

(2) Neglects turbulent flow and hysteresis loss in the electric motor.

(3) The currents in the electric motor are symmetrical three-phase sinusoidal currents.

In FOC algorithm, both the three-phase stator A-B-C coordinate system and the two-phase stator α-β coordinate system are the static coordinate systems. While the d-q coordinate system is revolving, the transforms between these three coordinates are given,

$$\begin{pmatrix} i_\alpha \\ i_\beta \end{pmatrix} = \sqrt{\frac{2}{3}} \begin{pmatrix} 1 & -\frac{1}{2} & -\frac{1}{2} \\ 0 & -\frac{\sqrt{3}}{2} & \frac{\sqrt{3}}{2} \end{pmatrix} \begin{pmatrix} i_a \\ i_b \\ i_c \end{pmatrix}, \tag{1}$$

$$\begin{pmatrix} i_d \\ i_q \end{pmatrix} = \begin{pmatrix} \cos\theta & \sin\theta \\ -\sin\theta & \cos\theta \end{pmatrix} \begin{pmatrix} i_\alpha \\ i_\beta \end{pmatrix}, \tag{2}$$

where i_a, i_b, i_c—a-, b- and c-axis armature currents,
i_d, i_q—d- and q-axis armature currents,
i_α, i_β—α- and β-axis armature currents,
θ—Rotor phase.

The torque of the PMSM is determined by i_d and i_q,

$$T_e = P_n \psi_a i_q + P_n (L_d - L_q) i_d i_q, \tag{3}$$

where L_d, L_q—d- and q-axis inductances,
P_n—Number of pole pairs,
Ψ_a—Permanent magnet flux-linkage,
T_e—Output torque.

In this study, a surface-mounted PMSM for which L_d equals to L_q, is used. Hence Eq. (3) can be simplified as:

$$T_e = P_n \psi_a i_q = K i_q. \tag{4}$$

The hysteresis PWM current control shown in Fig. 1 is a part of the FOC algorithm, and it is also known as bang-bang control, which is separately performed in the three phases. Each controller determines the switching-state of one inverter's half-bridge in such a way that the corresponding current is maintained within a hysteresis band h_0[24]. Hysteresis band h_0 corresponds to the response time and the stability of the current control. A small h_0 brings an accurate control effect, but it increases the instability of the control strategy.

The basic parameters of the I-PMSM used in this study are shown in Table 1. The FOC control algorithm is shown in Fig. 2.

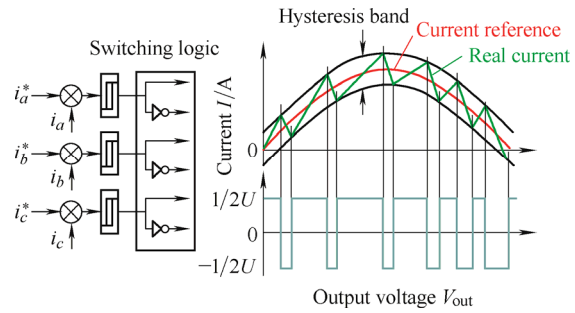

Fig. 1.　Hysteresis PWM current control and switching logic

Table 1.　Basic parameters of the I-PMSM

Parameter	Value
Number of poles P_n	4
Timer frequency f_{timer}/kHz	10
Q-, d-axis stator inductance L_d, L_q/mH	8.5
Stator phase resistance R_s/Ω	0.2
Typical hysteresis band h_0/A	0.1
Torque constant K/(N • m • A^{-1})	6.037 5
Rotor inertia J_{Rotor}/(kg • m^2)	0.2

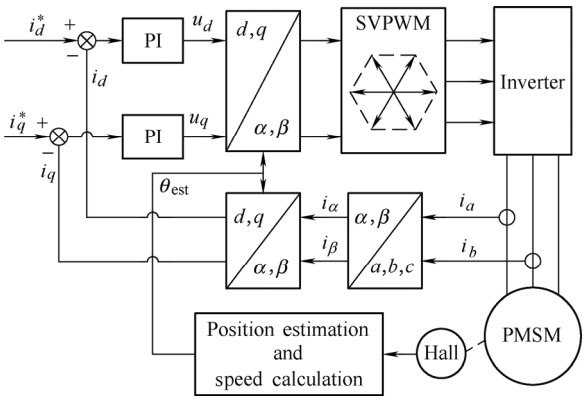

Fig. 2.　Control diagram of FOC for I-PMSM

2.2　Model of drive wheel dynamics

The drive wheel model comprises the I-PMSM and a two-inertia tire model. The tire sidewall's torsional linear stiffness and damping coefficients are denoted as K_r and C_r, respectively. Actually, the stiffness and damping coefficients are non-linear, however, the tire operates in a narrow frequency range in the simulation situation adopted in this paper. Thus these parameters can be assumed to be linear. The schematic for this model is shown in Fig. 3[14].

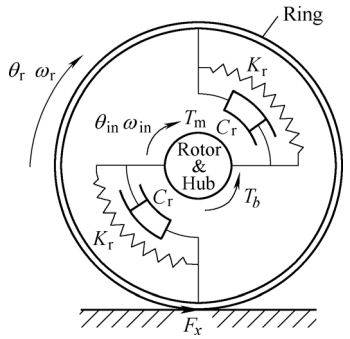

Fig. 3.　Drive wheel dynamics model

Considering a quarter car model along with the above I-PMSM/tire and treat/road friction models, the equations describing the entire system are reduced to the following:

$$(J_{Hub}+J_{Rotor})\ddot{\theta}_{in}=T_e-K_r(\theta_{in}-\theta_r)-C_r(\dot{\theta}_{in}-\dot{\theta}_r), \quad (5)$$

$$J_{Ring}\ddot{\theta}_r=K_r(\theta_{in}-\theta_r)+C_r(\dot{\theta}_{in}-\dot{\theta}_r)-F_x r. \quad (6)$$

where　J_{Hub}, J_{Rotor}, J_{Ring}—Hub, rotor and ring inertias,
θ_{in}, θ_r—Rotor/hub and ring angular positions,
$\dot{\theta}_{in}$, $\dot{\theta}_r$—Rotor/hub and ring rotary speeds,
$\ddot{\theta}_{in}$, $\ddot{\theta}_r$—Rotor/hub and ring accelerations.

The tire/road contact interface (a uniform high-μ surface) is described by the magic formula pragmatic model and non-linear relaxation length-based model. Only longitudinal motion of the vehicle is considered in this paper. On this premise, the Magic Formula pragmatic model indicating the relationship between slip ratio s_x and steady longitudinal force F_x^S is given:

$$s_x=\frac{\dot{\theta}_r r-V}{V}, \quad (7)$$

$$F_x^S=D\sin[C\arctan(Bs_x-E(Bs_x-\arctan Bs_x))]. \quad (8)$$

where　r—Effective rolling radius of tire,
V—Vehicle velocity,
B—Stiffness factor,
D—Peak factor,
E—Curvature factor.

Parameters B, D, and E were measured experimentally and related to the vertical load, as shown in Eqs. (9)–(11)[12]:

$$C=1.685,\ E=0.344, \quad (9)$$

$$D=\frac{4840}{(1+V/16.67)}, \quad (10)$$

$$B=\frac{86\,040}{[8155.4/(1+V/16.67)+0.1]}. \quad (11)$$

Fig. 4 shows the typical F_x^S–s_x relationship under different road conditions.

Only the steady force description cannot give a precise summary of the longitudinal force response. The measurement shows that the dynamic reaction of the tire force to disturbances can be approximated well using the first order system. The non-linear relaxation length-based model is used to describe the dynamic longitudinal force F_x^D derived from the steady longitudinal force.

$$\tau\dot{F}_x^D+F_x^D=F_x^S. \quad (12)$$

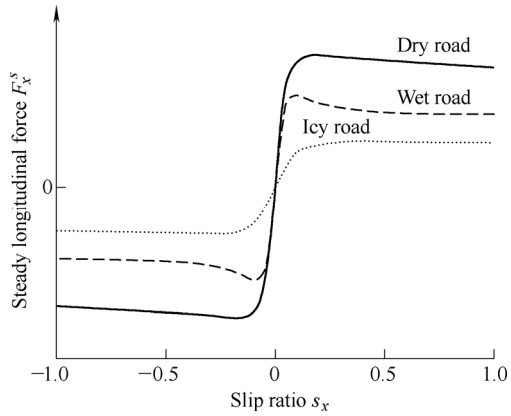

Fig. 4. Typical F_x^s-s_x curves for different road conditions

The time constant τ can be derived from the relaxation length r_x as follows:

$$\tau = \frac{r_x}{r\dot{\theta}_r}. \tag{13}$$

The relaxation length is the function of the slip ratio s_x and the wheel load F_z, but the detailed function is too complex to be used in the simulation. Thus a 2D look-up table revealing the relationship between the computed relaxation length and various values of F_z, as well as s_x is appropriate to be adopted, as presented in Fig. 5[14]. In this study, to minimize the complexity of the calculation process, the non-linear characteristics of the contact patch which is indicated by the speed difference between the leading and trailing parts is ignored.

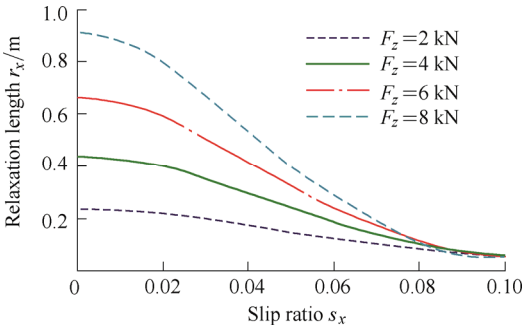

Fig. 5. Computed relaxation length characteristics

Finally, a typical passenger vehicle is chosen and the kinetic equations of the quarter vehicle can be established:

$$F_f = \frac{Mg}{4}(0.007\,6 + 0.000\,2V) + 0.25\frac{C_D A V^2}{5.875}, \tag{14}$$

$$\dot{V} = \frac{F_x^D - F_f}{(M/4)}. \tag{15}$$

where F_f—Drag resistance,
M—Vehicle mass,
C_D—Drag coefficient,
A—Wind area.

The basic parameters in Eqs. (5)–(15) are listed in Table 2. To point out, the dynamic stiffness and damping coefficients of the tire are difficult to measure, while the static values can be measured via modal experiments. However, the static ones appear to be less than the dynamic ones; furthermore, the stiffness and damping coefficients vary over a wide range of values (for example, K_r=10 kN • m/rad, C_r=40 N • m • s/rad in Ref. [25]; K_r=19 438 N • m/rad, C_r=4 N • m • s/rad in Ref. [14]) depending on different tire states (e.g., tire pressure). To emphasize the vibration in tire deformation, tires with several different parameters are chosen to show their different performance and the standard parameters are chosen to be within reasonable ranges according to the existing studies[14, 25].

Table 2. Basic parameters of vehicle model

Parameter	Value
Hub inertia J_{Hub}/(kg • m^2)	0.3
Ring inertia J_{Ring}/(kg • m^2)	0.8
Torsional stiffness K_r/(kN • m • rad^{-1})	12
Damping coefficient C_r/(N • m • s • rad^{-1})	10
Effective rolling radius r/m	0.313
Vehicle mass M/kg	1600
C_DA/m^2	0.6

3 Effect of Various System Parameters

In this section, the parameters sensitivity, including mass distribution ratio of the drive wheel α (which is defined in Eq. (16)), the tire torsional stiffness K_r, the tire damping coefficient C_r, and the hysteresis band h_0, on slip ratio estimation and tire torsional vibrations is studied. The simulation conditions that were employed specify that the quarter car with an initial speed of 2 m/s is started on a flat and high-μ road (μ=1) under the torque curve shown in Fig. 6.

$$\alpha = \frac{J_{Hub} + J_{Rotor}}{J_{Ring}}. \tag{16}$$

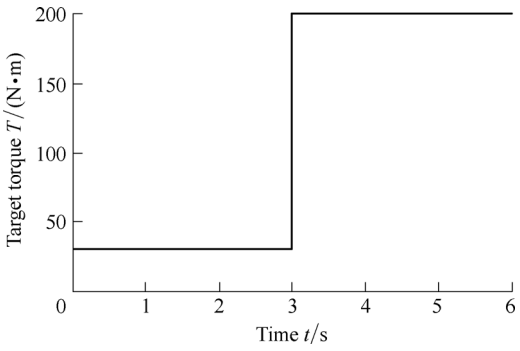

Fig. 6. Torque curve in the simulation

3.1 Relative error of slip estimation

In practical applications, the slip ratio (traction mode) is calculated using the rotor/hub rotary speed rather than the

ring rotary speed as shown in Eq. (17):

$$s_x' = \frac{\dot{\theta}_{in} r - V}{V}. \tag{17}$$

This will introduce significant errors during the instantaneous dynamic process because there is a difference between the two rotary speeds discussed above. The estimation error of slip ratio varies with different parametric combinations and the average relative error of slip ratio estimation is defined as:

$$e_{slip}\% = \frac{100}{t_2 - t_1} \int_{t_1}^{t_2} \frac{|s_x' - s_x|}{s_x} dt\%, \tag{18}$$

where t_1 and t_2 are used to select the acceleration region. To estimate the slip ratio estimation error caused by the significant tire deformation, t_1 and t_2 are set to 3 s and 5 s, respectively, because the torque changes from 30 N • m to 200 N • m at 3 s and the vehicle is severely accelerated since 3 s. K_r and C_r are the main structural parameters of the tire. The influence of these two parameters on the slip ratio estimation is shown in Fig. 7.

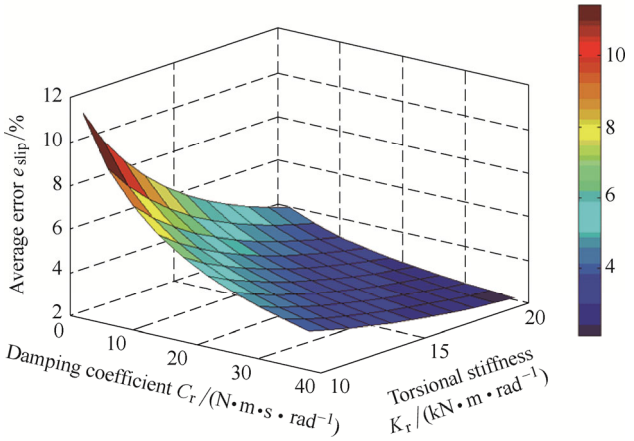

Fig. 7. Influence of various C_r and K_r on slip ratio estimation

As C_r and K_r increase, the average error of slip ratio estimation decreases, namely, the estimation error will disappear when the tire is rigid. However, there is an obvious average error (about 8%) for a typical tire (K_r=12 kN • m/rad, C_r=10 N • m • s/rad) during the abrupt acceleration process from 3 s to 5 s. Thus the tire's transient dynamic performance should be taken into account to accurately estimate the slip ratio in practical applications.

Fig. 8 gives the simulation results, which indicate the effect of various α and h_0 on the slip ratio estimation. The different hysteresis band h_0 has small fluctuations, but it generally has no obvious effect on the estimation of slip ratio. Nonetheless, the mass distribution ratio α of the drive wheel significantly affects the slip ratio estimation. In this simulation, the sum of hub, rotor, and ring inertia values remain constant while α changes. It is clear that the estimation result of slip ratio derived from $\dot{\theta}_{in}$ has a smaller error when the wheel mass aggregates to the center of tire (α increases), as shown in Fig. 8. Moreover, the estimation error can be kept within a small range when the mass distribution of the drive wheel is well matched (α is about 0.7 as shown in Fig. 8). When the mass spreads to the ring, the estimation error of the silp ratio increases dramatically. In conclusion, the I-PMSM and tire should be carefully matched before use. In addition, the rotor inertia can be increased to ensure a high slip ratio estimation accuracy if no experiments and calibration are possible.

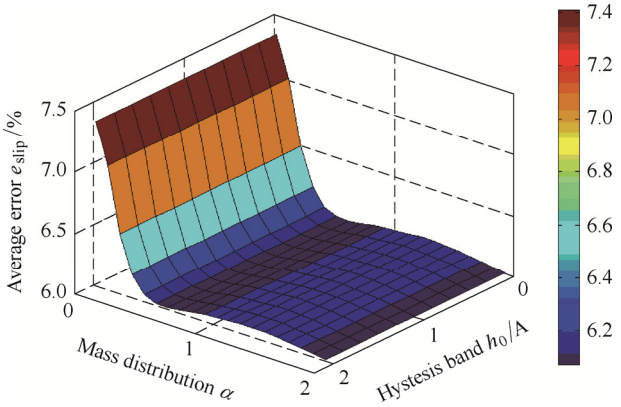

Fig. 8. Influence of various α and h_0 on slip ratio estimation

The estimation error of slip ratio is due to the drive wheel's transient processes when the ring rotary speed is used in the calculation. The average error of slip estimation decreases as C_r and K_r increase. In addition, the mass distribution of the drive wheel should be appropriate because α will also significantly affect the slip ratio estimation. The drive wheel model adopted in this paper can be used as a feedforward module to compensate the estimation error by using a multivariate look-up table, as shown in Fig. 7 and Fig. 8.

3.2 Tire torsional and longitudinal vibrations

It has been verified by the modal analysis and experiments that the tire torsional vibrations generated during acceleration bring significant noise as well as change the tire shape[25]. Further, the vibration in the driveline are dramatically affected by the drive wheel parameters. The longitudinal vibration directly corresponds to the longitudinal force F_x, and the torsional vibration can be measured by the angular difference between the hub/rotor and ring as Eq. (19) shows. These two measurable variables, which can be clearly seen in frequency domain, reflect the higher flexible deformation of tire. For this reason, a parameter study is performed, focusing on the influence of the mass distribution ratio α, torsional stiffness K_r, and damping coefficient C_r.

$$\Delta\theta = \theta_{in} - \theta_r, \tag{19}$$

First, simulation focusing on α is carried out, as shown in Fig. 9.

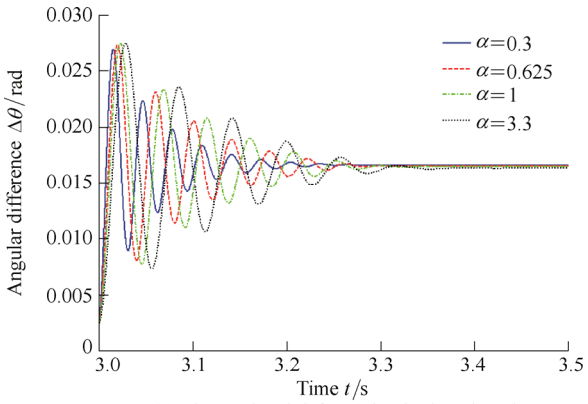

(a) Tire torsional deformation in time domain

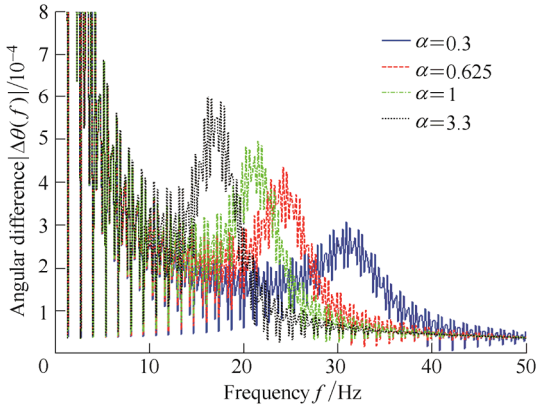

(b) Tire torsional deformation in frequency domain

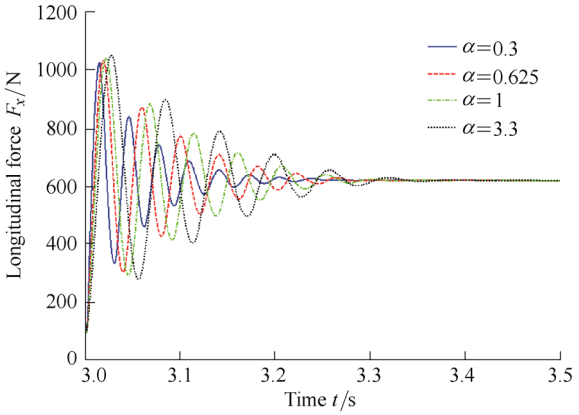

(c) Longitudinal force in time domain

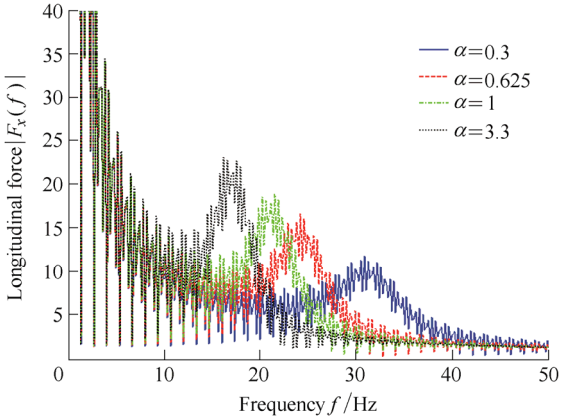

(d) Longitudinal force in frequency domain

Fig. 9. Influence of various α on drive wheel vibrations

The simulation produced similar results for the torsional vibration and longitudinal vibration. Figs. 9(b) and 9(d) were derived using the fast Fourier transform (FFT) process. As α increases, meaning that the wheel mass is centralized on the wheel center, the resonant frequencies of both the torsional vibration and longitudinal vibration increased, while the vibration amplitude decreased. The resonant frequency of a typical drive wheel (α=0.625) is about 24 Hz. Fig. 9 demonstrates the strong impact of the mass distribution on the frequency and amplitude of the vibration for which all the resonant frequencies are less than 50 Hz. This means that all of the vibrations are in the low frequency region; however, they cannot be neglected. Reducing the central mass of the drive wheel may decrease the vibration amplitude, leading to improved drivability of the vehicle.

Fig. 10 illustrates the influence of the torsional stiffness K_r on the vibration of drive wheel. Figs. 10(a) and 10(b) show that the frequency of torsional vibration increases with an increase in K_r, furthermore, a large K_r can suppress the vibration amplitude. It is clear that the torsional vibration will disappear if the tire is rigid. Figs. 10(c) and 10(d) show the longitudinal vibrations in the time and frequency domains, indicating that the frequency of longitudinal vibration increased with increasing K_r, while the vibration amplitude remained almost constant. The resonant frequency of the drive wheel, with K_r being within a reasonable range, was about several dozen Hertz.

Finally, the influence of the damping coefficient C_r is shown in Fig. 11. The frequency of the torsional vibration and longitudinal vibration remain constant even with varying C_r. However, the vibration amplitude will increase when C_r decreases. The reason for this is that the damping coefficient is much less than the stiffness coefficient, so the resonant frequency of the drive wheel is determined mainly by K_r. However, C_r still has a significant influence on the vibration amplitude of the drive wheel. To suppress the vibration, C_r should be maintained above a specific value.

In summary, it is confirmed that the frequency of the vibration depends only on K_r and α (more parameters were considered, but the results were not included here). The vibration amplitude of the drive wheel is significantly influenced by C_r, K_r, and α. If these parameters are within reasonable ranges, the resonant frequency of the drive wheel will be less than 50 Hz. This conclusion is very important to judge if the noise/vibration results from the drive wheel when the NVH problem of the vehicle is analyzed in frequency domain.

4 Influence of Different Torque Curves

When the vehicle control unit (VCU) receives the pedal signal given by the driver, VCU will translate this pedal signal to the torque demand, and will then send it to the motor control unit (MCU). Different target torque curves indicate different pedal translations, which lead to different

control effects. Therefore, it is important to carry out a qualitative investigation into the optimization of the target torque curve in a wheel-independent-drive EV. Four different curves, including a step torque change, a ramp torque change, a sine torque change and a parabola torque change at 3 s, were chosen for comparison purposes, and a typical drive wheel is used in this section. Fig. 12 shows the four target torque curves.

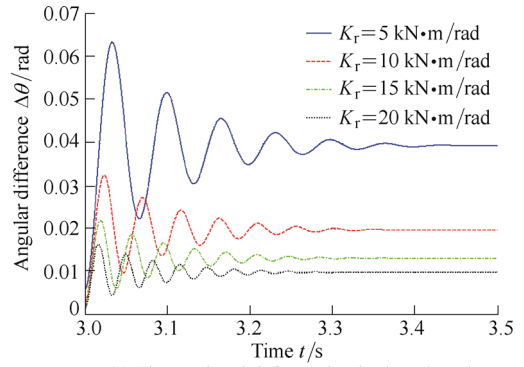

(a) Tire torsional deformation in time domain

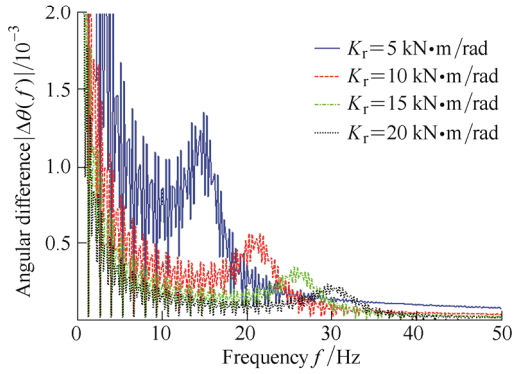

(b) Tire torsional deformation in frequency domain

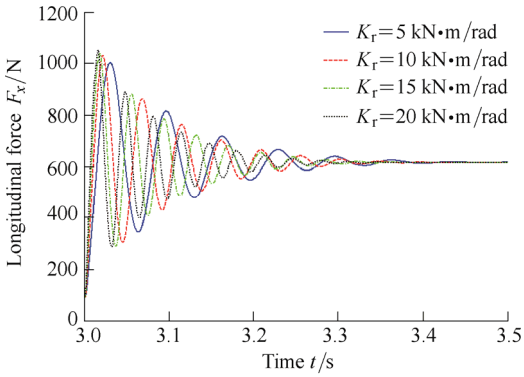

(c) Longitudinal force in time domain

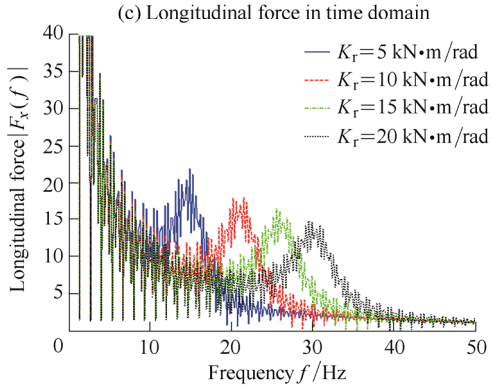

(d) Longitudinal force in frequency domain

Fig. 10.　Influence of various K_r on drive wheel vibrations

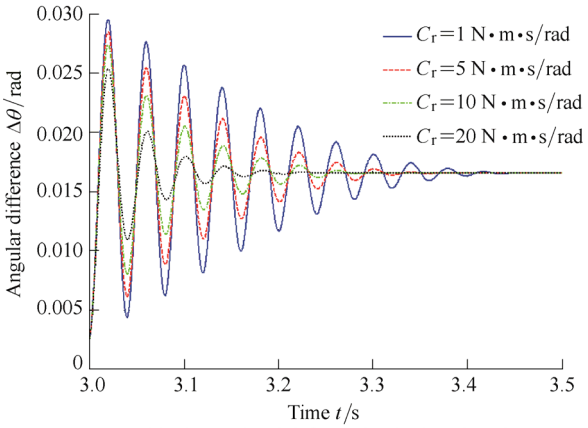

(a) Tire torsional deformation in time domain

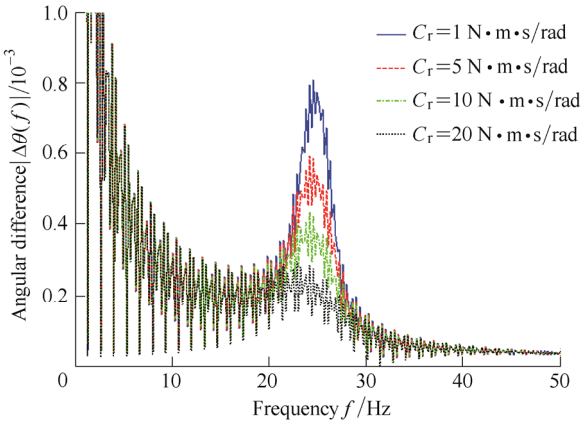

(b) Tire torsional deformation in frequency domain

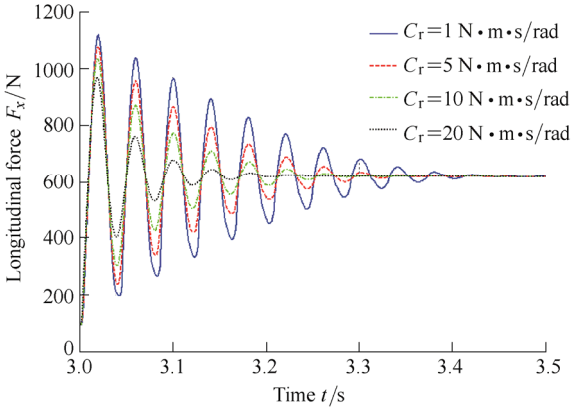

(c) Longitudinal force in time domain

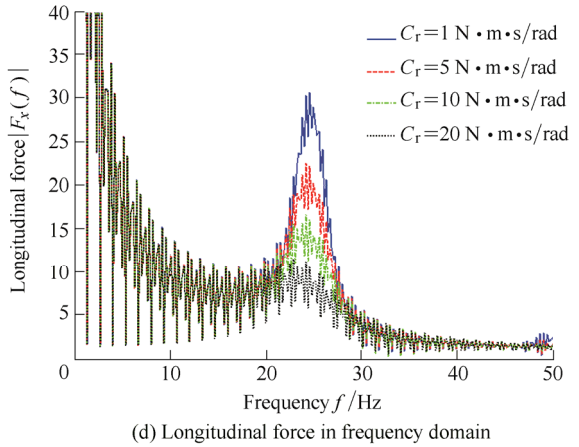

(d) Longitudinal force in frequency domain

Fig. 11.　Influence of various C_r on drive wheel vibrations

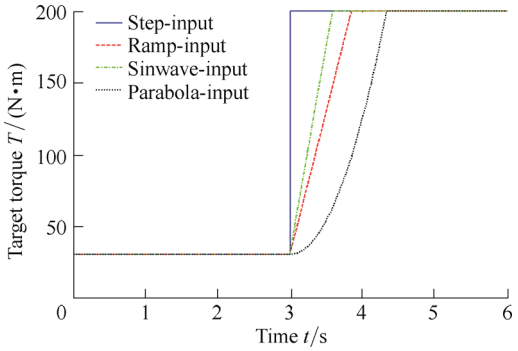

Fig. 12. Four different torque curves

The average estimation errors of the slip ratio under four torque curves are compared and shown in Fig. 13. It can be seen that the parabola torque input causes the smallest estimation error, while the step input causes the largest error among the four torque inputs. The estimation error of the slip ratio gets violent with increasing changes in the speed of the torque. Therefore, the increase rate of the torque should be controlled to within a reasonable limit especially at the beginning of the acceleration process. Additionally, the increase rate can be adjusted to a larger value in the middle or the later periods of the acceleration, as seen in the parabola torque curve. Translating the driver demand based on this principle can reduce the vibration in the driveline of a wheel-independent-drive EV.

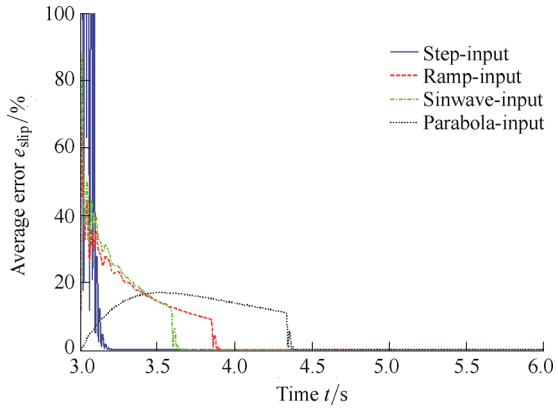

Fig. 13. Slip ratio estimation error under different torque curves

Different target torque curves also lead to disparate tire vibration effects, as shown in Fig. 14. The vibrations in the longitudinal force and tire deformation have similar characteristics, and are obvious for varying step torque conditions, while the other three results show hardly any vibrations. In conclusion, the vibration occurs only when the torque input is sufficiently fast. This convinces that it is a new problem which is not present in conventional vehicles because the motor torque response is much faster than that of an engine (about 50 times faster). To limit the speed with which the torque changes, a low-pass filter or an average filter can be used in the pedal position translation process once the motor torque response satisfies the driver acceleration demand.

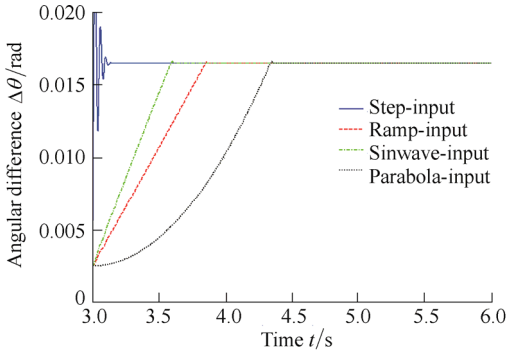

(a) Tire torsional deformation

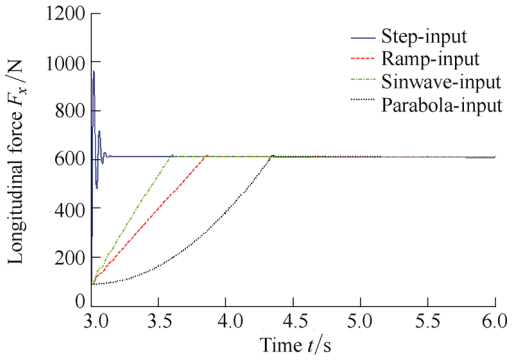

(b) Longitudinal force

Fig. 14. Longitudinal and torsional vibrations under different torque curves

5 Conclusions

(1) The drive wheel, with respect to the transient behavior of an I-PMSM and a tire, is modeled in this paper. This model is near-real and appropriate for studying the effect of parameter sensitivity on the slip ratio estimation.

(2) The effect of K_r, C_r, α and h_0 on the average error of slip ratio estimation under surge torque change condition has been examined, showing that a higher K_r, C_r, and an appropriate α result in a smaller estimation error when the rotary speed of the tire ring is used in the slip ratio calculation.

(3) Different parameters have different effects on drive wheel vibrations. For example, the damping coefficient C_r has no relationship with the vibration frequency; however, it significantly affects the vibration amplitude. Also as α and K_r increase, the vibration frequency increases and the vibration amplitude decreases. Generally, the vibration frequency is below 50 Hz and is not negligible.

(4) Different target torque curves are compared and the results show that the estimation error of slip ratio increases for increasing torque input speeds. Moreover, the driveline vibration only occurs when the torque input is sufficiently fast. This is important to use a low-pass filter or an average filter in the translation of the pedal signal to the required motor torque.

References

[1] XU Yanliang, XU Jiaqun, WAN Wenbin, et al. Development of permanent magnet synchronous motor used in electric vehicle[C]//

Electrical Machines and Systems. IEEE Proceedings of the Fifth International Conference on. ICEMS 2001, Shenyang, China, August 18–20, 2001: 884–887.

[2] WALLMARK O, HAMEFORS L, CARLSON O. Control algorithms for a fault-tolerant PMSM drive[J]. *IEEE Transactions on Industrial Electronics*, 2007, 54(4): 1973–1980.

[3] GULEZ K, ADAM A A, PASTACI H. Torque ripple and EMI noise minimization in PMSM using active filter topology and field-oriented control[J]. *IEEE Transactions on Industrial Electronics*, 2008, 55(1): 251–257.

[4] FUJIMOTO H, TSUMASAKA A, NOGUCHI T. Direct yaw-moment control of electric vehicle based on cornering stiffness estimation[C]//*31st Annual Conference of the IEEE Industrial Electronics Society*, North Carolina, USA, November 6–10, 2005: 2626–2631.

[5] KIM J, KIM H. Electric vehicle yaw rate control using independent in-wheel motor[C]//*Power Conversion Conference*, Nagoya-shi, Japan, April 2–5, 2007: 705–710.

[6] SAKAI S, SADO H, HORI Y. Motion control in an electric vehicle with 4 independently driven in-wheel-motors[J]. *IEEE/ASME Transaction Mechatronics*, 1999, 4(1): 9–16.

[7] CANUDAS-DE-WIT C, OLSSON H, ASTROM K J, et al. A new-model for control of systems with friction[J]. *IEEE Transactions on Automatic Control*, 1995, 40(3): 419–425.

[8] TSOTRAS A, MAVROS G. Frictional contact behavior of the tyre: the effect of tread slip on the in-plane structural deformation and stress field development[J]. *Vehicle Systems Dynamics*, 2010, 48(8): 891–921.

[9] VELENIS E, TSIOTRAS P, CANUDAS-DE-WIT C, et al. Dynamics tire friction models for combined longitudinal and lateral vehicle motion[J]. *Vehicle System Dynamics*, 2005, 43(1): 3–29.

[10] CANUDAS-DE-WIT C, TSIOTRAS P, VELENIS E, et al. Dynamic friction models for Road/Tire longitudinal interaction[J]. *Vehicle System Dynamics*, 2003, 39(3): 189–226.

[11] RILL G. First order tire dynamics[C]//*Proceedings of the 3rd European Conference on Computational Mechanics Solids, Structures and Coupled Problems in Engineering*, Lisbon, Portugal, June 5–8, 2006: 1–9.

[12] PACEJKA H B. *Tyre and vehicle dynamics*[M]. Oxford: Butterworth-Heinemann, 2002.

[13] PAUWELUSSEN J P, GOOTJES L, SCHRODER C, et al. Full vehicle ABS braking using the swift rigid ring tyre model[J]. *Control Engineering Practice*, 2003, 11(2): 199–207.

[14] ADCOX J, AYALEW B, RHYNE T, et al. Interaction of anti-lock braking systems with tire torsional dynamics[C]//*Meeting of the Tire Society*, Akron, USA, September 13–14, 2011: 1–18.

[15] MASTANDREA M, VANGI D. Influence of braking force in low-speed vehicle collisions[J]. *Proc IMechE Part D: J Automobile Engineering*, 2005, 219: 151–164.

[16] FUJII K, FUJIMOTO H. Traction control based on slip ratio estimation without detecting vehicle speed for electric vehicle[C]// *Proc. 4th Power Convers. Conf.*, Nagoya, Japan, April 2–5, 2007: 688–693.

[17] FUJII K, FUJIMOTO H. Slip ratio estimation and control based on driving resistance estimation without vehicle speed detection for electric vehicle[J]. *The Society of Instrument and Control Engineers*, 2007, 084-1-3: 1–6.

[18] ZHAO Yane, ZHANG Jianwu. Modeling and simulation of electronic differential system for an electric vehicle with two-motor-wheel drive[J]. *International Journal of Vehicle Systems Modelling and Testing*, 2009, 4: 117–131.

[19] SYED F U, KUANG M L, HAO Ying. Active damping wheel-torque control system to reduce driveline oscillations in a power-split hybrid electric vehicle[J]. *IEEE Transactions on Vehicular Technology*, 2009, 58(9): 4769–4785.

[20] BARTRAM, MAVROS G, BIGGS S. A study on the effect of road friction on driveline vibrations[J]. *Proceedings of the Institution of Mechanical Engineers, Part K: Journal of Multi-body Dynamics*, 2010, 224(4): 321–340.

[21] MA Yan, ZHANG Kangkang, GU Jing, et al. Design of the control system for a four-wheel driven micro electric vehicle[C]// *Proceedings of 5th IEEE Vehicle Power and Propulsion Conference, VPPC '09*, Dearborn, MI, USA, September 7–10, 2009: 1813–1816.

[22] PILLAY P, KRISHNAN R. Modeling, simulation and analysis of permanent magnet motor drives-Part I: The permanent magnet synchronous motor drive[J]. *IEEE Transactions on Industry Applications*, 1989, 25(2): 265–273.

[23] DORRELL D G, NGU S S, COSSAR C. Comparison of high pole number ultra-low speed generator designs using slotted and airgap windings[J]. *IEEE Transactions on Magnetics*, 2012, 48(11): 3120–3123.

[24] CHATTERJEE A, CUSUMANO J P, ZOLOCK J D. On contact-induced standing waves in rotating tires: experimental and theory[J]. *Journal of Sound and Vibration*, 1999, 227(5): 1049–1081.

[25] ZEGELAAR P W A, PACEJKA H B. The in-plane dynamics of tyres on uneven roads[J]. *Vehicle System Dynamics*, 1996, 25(S1): 714–730.

Biographical notes

SONG Ziyou, born in 1989, is currently a PhD candidate at *State Key Laboratory of Automotive Safety and Energy, Tsinghua University, China*. He received his bachelor degree in Automotive Engineering from *Tsinghua University, China*, in 2011. His research interests include in-wheel PMSM control of electric vehicles and hybrid energy storage system optimization.
Tel: +86-10-6278-5706; E-mail: ziyou.song@qq.com

LI Jianqiu, born in 1972, is currently a professor at *Department of Automotive Engineering, Tsinghua University, China*. He received his PhD degree in power mechanism and engineering from *Tsinghua University, China*, in 2000. His research interests include electronic control of diesel engine, key technology of automotive electronics, fuel cell and powertrain control.
E-mail: lijianqiu@tsinghua.edu.cn

WEI Yintao, born in 1971, is currently a professor at *State Key Laboratory of Automotive Safety and Energy, Tsinghua University, China*. He received his PhD degree in Engineering Mechanics from *Harbin Institute of Technology, China*, in 1997. His research interests include tire dynamic modeling and control.
E-mail: weiyt@tsinghua.edu.cn

XU Liangfei, born in 1982, is currently an associate professor at *State Key Laboratory of Automotive Safety and Energy, Tsinghua University, China*. He received his PhD degree in Engineering Mechanics from *Tsinghua University, China*, in 2006. His research interests include energy management of HEVs, EVs and FCVs.
E-mail: xuliangfei@tsinghua.edu.cn

OUYANG Minggao, born in 1958, is currently a professor at *Department of Automotive Engineering, Tsinghua University, China*. He received his PhD degree in mechanical engineering from *Technical University of Denmark, Lyngby*, in 1993. His research interests include new energy vehicles, automotive powertrains, engine control systems, and transportation energy strategy and policy.
E-mail: ouymg@tsinghua.edu.cn